ACS APPLIED ELECTRONIC MATERIALS

Article

Cite This: ACS Appl. Electron. Mater. 2019, 1, 1408−1417

pubs.acs.org/acsaelm

Low-Cost One-Step Fabrication of Highly Conductive ZnO:Cl Transparent Thin Films with Tunable Photocatalytic Properties via Aerosol-Assisted Chemical Vapor Deposition

Arreerat Jiamprasertboon,[†,‡] Sebastian C. Dixon,[‡] Sanjayan Sathasivam,[‡] Michael J. Powell,[‡] Yao Lu,[§] Theeranun Siritanon,[†] and Claire J. Carmalt*[,‡]

[†]School of Chemistry, Institute of Science, Suranaree University of Technology, 111 University Avenue, Muang, Nakhon Ratchasima, 30000, Thailand

[‡]Materials Chemistry Centre, Department of Chemistry, University College London, 20 Gordon Street, London, WC1H 0AJ, U.K.

[§]Department of Mechanical Engineering, University College London, London, WC1E 7JE, U.K.

Supporting Information

ABSTRACT: Low-cost, high-efficiency, and high quality Cl-doped ZnO (ZnO:Cl) thin films that can simultaneously function as transparent conducting oxides (TCOs) and photocatalysts are described. The films have been fabricated by a facile and inexpensive solution-source aerosol-assisted chemical vapor deposition technique using NH_4Cl as an effective, cheap, and abundant source of Cl. Successful Cl_O substitutional doping in the ZnO films was evident from powder X-ray diffraction, X-ray photoelectron spectroscopy, and time-of-flight secondary ion mass spectrometry results, while scanning electron microscopy reveals the impact of Cl doping on the ZnO thin film morphology. All ZnO:Cl films deposited were transparent and uncolored; optical transmittance in the visible region (400−700 nm) exceeded 80% for depositions using 5−20 mol % Cl. Optimal electrical properties were achieved when using 5 mol % Cl with a minimum measured resistivity of $(2.72 \pm 0.04) \times 10^{-3}$ Ω·cm, in which the charge carrier concentration and mobility were measured at $(8.58 \pm 0.16) \times 10^{19}$ cm^{-3} and 26.7 ± 0.1 cm^2 V^{-1} s^{-1} respectively, corresponding to a sheet resistance (R_{sh}) of 41.9 Ω□$^{-1}$ at a thickness of 650 nm. In addition to transparent conducting properties, photocatalytic behavior of stearic acid degradation in the ZnO:Cl films was also observed with an optimal Cl concentration of 7 mol % Cl, with the highest formal quantum efficiency (ξ) measured at $(1.63 \pm 0.03) \times 10^{-4}$ molecule/photon, while retaining a visible transparency of 80% and resistivity $\rho = (9.23 \pm 0.13) \times 10^{-3}$ Ω·cm. The dual functionality of ZnO:Cl as both a transparent conductor and an efficient photocatalyst is a unique combination of properties making this a particularly unusual material.

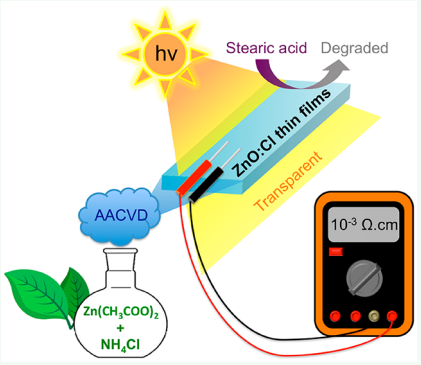

KEYWORDS: *doped ZnO, anion doping, transparent conducting oxides, photocatalysts, aerosol-assisted chemical vapor deposition, thin films*

INTRODUCTION

Sustainability is a progressively essential theme in the design and fabrication of materials where the environmental impact of producing materials is considered to be of key significance.[1] Thin film deposition plays an important role in a variety of technologies, e.g. flat-screen panels, photocatalysts, solar cells, batteries, and computing devices.[2] The ability to create and design thin film functional materials for such purposes necessitates the aim to produce materials with new, advanced, and multifunctional properties. In particular, materials that can simultaneously exhibit the behavior of both good transparent conducting oxides (TCOs) and good photocatalysts are rarely seen. A variety of factors affect these different functional properties, e.g. doping content, crystal defects, grain boundaries, crystallinity, surface microstructure, and film thickness.[3] TiO_2 has been the most studied material to date that exhibits the dual functionality of electrical conductivity and photocatalytic activity. In its undoped form, thin films of TiO_2 are transparent to visible light and exhibit photoactivity under UV irradiation but no electrical conductivity. When doped with e.g. Nb^{5+}, Ta^{5+}, or W^{5+} on Ti^{4+} sites or F^- on O^{2-} sites,[3−6] TiO_2 exhibits low electrical resistivity while maintaining photocatalytic activity. However, due to the high carrier concentration that is necessary to achieve low resistivity (× 10^{-3} Ω·cm) as required for electrode applications, the highly doped TiO_2 films often display a blue coloration (arising from Ti^{3+} states) and hence poor visible light transmittance.[7]

Received: March 25, 2019
Accepted: June 3, 2019
Published: June 3, 2019

DOI: 10.1021/acsaelm.9b00190
ACS Appl. Electron. Mater. 2019, 1, 1408−1417

Doped ZnO does not suffer from such issues. It is a wide band gap (~3.37 eV) semiconductor that displays excellent optoelectronic properties that are improved by doping with a variety of ions such as Al, Ga, and In on Zn sites and F on O sites without the loss of transparency due to coloration.[8,9] Anion doping in particular has advantages over cation doping, due to the anion effecting little perturbation of the conduction band (CB) compared with cation doping, which plays an important role in minimizing the electron scattering in the CB and therefore maximizing electron transport and conductivity. Meanwhile, creation of a carrier donor level close to the CB minimum (CBM) enables retention of the material's wide band gap and therefore transparency.[10] Doping ZnO with F has gained much attention, likely due to the success of the more widely known F-doped SnO_2. However, doping ZnO with other anions such as Cl has not been widely investigated in spite of some promising properties recently reported.[11−16] ZnO also displays photocatalytic properties, and various metals (e.g., Ag, Al, Sn) and nonmetals (e.g., C, N, S) have been investigated to improve its photocatalytic performance for pollutant degradation such as organic dyes.[17]

Thin films of ZnO can be grown using a variety of techniques as sputtering,[18] pulsed laser deposition,[19] spin coating,[20] atomic layer deposition (ALD),[21] and chemical vapor deposition (CVD).[22−25] Aerosol assisted chemical vapor deposition (AACVD) in particular holds some distinct advantages when compared with the aforementioned alternatives.[26] It is a simple thin film deposition process requiring minimal apparatus, whose primary requisite for precursor selection is solubility in one of a range of common organic solvents such as toluene or methanol, thus vastly expanding the scope of starting materials from the volatile precursors required for conventional or atmospheric pressure CVD.[22−27] Without the need for toxic or volatile precursors, it is considered as a highly sustainable and scalable route to thin film deposition.[1] Interestingly, the morphology and particle size of films deposited via AACVD are tunable with the choice of solvent, deposition temperature, and the frequency of the ultrasonic humidifier; therefore, there is a significant degree of control over film properties.[26,27] Moreover, the mass transport rate of precursors by the aerosol route is high[28] compared to classical reduced-pressure CVD routes providing a high deposition rate,[29] drawing a comparison with the better established thermal atmospheric-pressure CVD without the need for precursors with high vapor pressure.[30] Thus, with its high growth rates and the need for vacuum deposition and limited volatile precursor selection eliminated, the AACVD technique has potential for widespread industrial scale.[31,32]

Recently, ZnO:Cl thin films synthesized by the AACVD method using $FeCl_3$ as a Cl source were reported.[33] The exploration of its dual functionality as both a photocatalyst and a TCO is of great interest. In the previous work, Cl-doping resulted as a side reaction from decomposition of $FeCl_3$;[33] however, here we have used NH_4Cl to provide a cheaper and cleaner deposition route to highly efficient ZnO:Cl without the need to dispose of Fe-based precipitates, providing an efficient Cl source while enabling strong tunability between the multifunctional transparent conducting and photocatalytic behaviors of ZnO:Cl. Films deposited from NH_4Cl have enhanced TCO properties compared to those deposited using $FeCl_3$ and are photocatalytically active with the optimum amount of Cl doping.

EXPERIMENTAL SECTION

Film Synthesis. All ZnO:Cl films were obtained using aerosol assisted chemical vapor deposition (AACVD). High purity chemicals Zn(II) acetate dihydrate, $Zn(CH_3COO)_2{\cdot}2H_2O$ (≥98%, Sigma-Aldrich), and ammonium chloride, NH_4Cl, were used as precursors. Methanol (99.9%, Fisher Scientific) was used as a solvent. Nitrogen (99.99%, BOC) was used as a carrier gas. The precursor solution was prepared by dissolving $Zn(OAc)_2{\cdot}2H_2O$ (0.50 g, 2.28 mmol) in methanol (20 mL). NH_4Cl was dissolved in methanol and then added to the solution in 0, 1, 3, 5, 7, 10, and 20 mol % quantities relative to Zn. Each solution was stirred thoroughly (*ca.* 10 min). Float glass with a 50 nm silica barrier layer was obtained from NSG Pilkington Ltd. and used as substrates cut to dimensions of 45 mm × 100 mm × 3.2 mm, and then cleaned using detergent, isopropanol, and acetone prior to use. The SiO_2 barrier layer is important to prevent leaching of ions from the substrate into the film. The substrate was put atop a carbon heating block, which was enclosed within a quartz tube. A top plate of stainless steel (48 mm × 150 mm) was suspended approximately 8 mm above the substrate to assist with the laminar flow of the gas carrying the aerosol. The schematic illustration of the AACVD setup was described in our previous work.[33] In the deposition, the prepared precursor solution was atomized using a "Liquifog" piezo ultrasonic humidifier (Johnson Matthey). The generated aerosol or mist was transported to the heated substrate through a brass baffle via nitrogen carrier gas with a flow rate of 1.5 L/min. The deposition was carried out at 500 °C until the solution had been fully atomized (*ca.* 15−20 min). The film-coated substrate was cooled down under a continuous flow of nitrogen gas and removed when the temperature of the reactor was lower than 100 °C. The film was cut into 1 × 1 cm^2 coupons for characterization.

Film Characterizations. XRD patterns were collected with a 2θ range of 10°−66° with a step size of 0.05° by a scan rate of 4 s/step using a Bruker-Axs D8 X-ray diffractometer with parallel beam optics equipped with a PSD LynxEye silicon strip detector. Monochromatic Cu $K_{\alpha1}$ and $K_{\alpha2}$ (λ = 1.54056 and 1.54439 Å, respectively), with an intensity ratio of 2:1, were generated using a voltage of 40 kV and a current of 40 mA. The incident beam angle was kept at a grazing incidence of 1°. Le Bail refinement using GSAS and EXPGUI software was carried out to obtain the cell parameters.[34,35] X-ray photoelectron spectroscopy (XPS) at the Zn 2p, O 1s, and Cl 2p peaks was used for elemental analysis. A Thermo Scientific K-alpha spectrometer with monochromatic Al Kα radiation, a dual beam charge compensation system, and a constant pass energy of 50 eV was utilized. The collected spectra were fitted using CasaXPS software. The C 1s peaks at 284.5 eV were used as reference for binding energy calibration. Time of flight secondary ion mass spectrometery (ToF-SIMS) coupled with depth profile analysis was used to probe the elemental composition of films. The measurement was performed on an ION-TOF 5 ToF-SIMS instrument. The analysis beam was 25 keV Bi^{3+}, and the sputter beam was 1 keV Cs^+ with a beam current of 65 nA. The sputter beam was rastered over a 300 × 300 μm^2 area and 200 × 200 μm area and the bismuth analysis beam was rastered over a 70 × 70 μm^2 area and 50 × 50 μm^2 area at the center of the sputtered region for undoped ZnO and ZnO:Cl films, respectively. Scanning electron microscope (SEM) images were gained to study the surface morphology and side-on SEM images were used to gain the film thickness using a JEOL JSM-6301F Field Emission instrument with an operated acceleration voltage of 10 kV. Surface topology and roughness (root mean squared, R_q) measurements were carried out on an atomic force microscope (AFM, Bruker Multimode 8). The tips were used in the ScanAsyst tapping mode to scan the area of 1.0 μm × 1.0 μm with 512 scans. UV/vis transmittance spectra were recorded to obtain the optical properties on a PerkinElmer Lambda 950 UV/vis/NIR spectrophotometer. Photoluminescence spectra were obtained by a Renishaw inVia Raman miscroscope using a 325 nm laser as the excitation light source.

The electrical properties including resistivity (ρ), carrier concentration (n), and carrier mobility (μ) were determined using Hall effect measurements in the Van der Pauw geometry using an Ecopia HMS-3000. A magnetic field of 0.58 T and an input current of 1 μA to 1 mA were applied for the measurement.

DOI: 10.1021/acsaelm.9b00190
ACS Appl. Electron. Mater. 2019, 1, 1408−1417

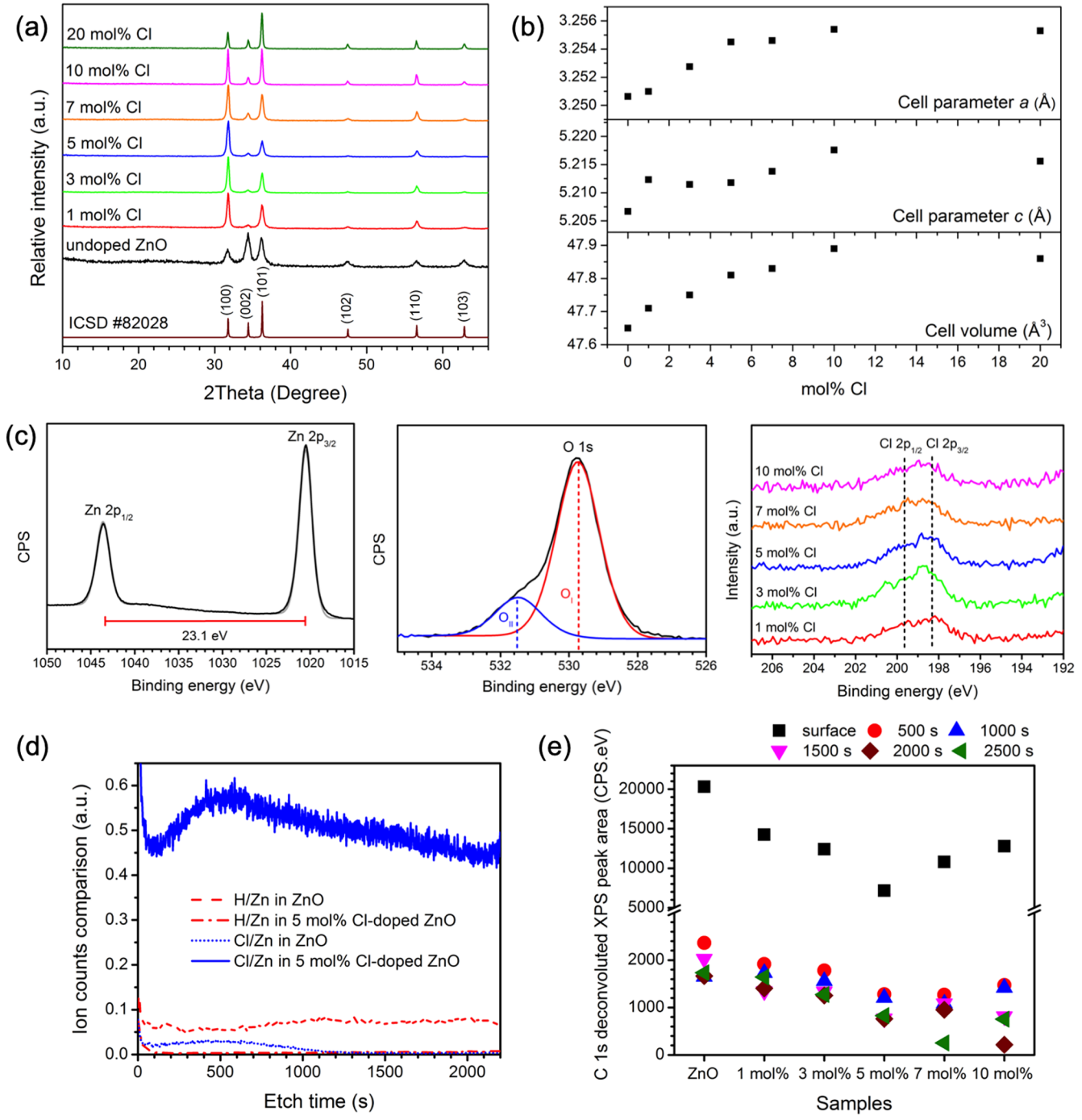

Figure 1. Synthesized ZnO:Cl films were characterized by several techniques. (a) XRD patterns for pure and Cl-doped ZnO thin films, which can be indexed as a single phase of wurtzite ZnO structure using simulated bulk ZnO (ICSD #82028). (b) Cell parameters *a*, *c* and cell volume of ZnO:Cl films. The increase in cell parameters indicates Cl substitution at O site. (c) High-resolution XPS spectra of Zn 2p and O 1s of 10 mol % Cl-doped ZnO and Cl 2p of a range of Cl-doped ZnO films. (d) The comparison content of H/Zn and Cl/Zn for undoped and 5 mol% Cl-doped ZnO films, which were determined by SIMS technique. (e) The C 1s XPS deconvoluted peak area obtained on surface and under etching (500 s, 1000 s, 1500 s, 2000 s, and 2500 s), corresponding to higher amount of C contamination in undoped ZnO film.

The test of stearic acid degradation under UVA illumination was used to investigate the photocatalytic properties. The films were cleaned by isopropanol and acetone and dipped in a stearic acid solution (0.05 M) in chloroform to create a thin layer of stearic acid before placed under UVA irradiation. To investigate the C−H bond decomposition in stearic acid, Fourier transform infrared (FTIR) spectra, with the absorbance mode in the range of 2700−3000 cm^{-1}, were collected using a PerkinElmer RX-I instrument. UVA (λ = 365 nm) light exposure was performed using a 5 × 18 W blacklight-bulb (BLB) UVA lamp (Phillips) with irradiation of 1 ± 0.1 mW cm^{-2} as measured using a UVX meter (UVP). A formal quantum efficiency (ξ) value was used to present the photocatalytic performance.

RESULTS AND DISCUSSION

Film Synthesis. Zn(II) acetate dihydrate[31] is a good precursor to fabricate ZnO films because it has relatively low toxicity and is inexpensive, easy to handle, and readily soluble in methanol. Other commonly used ZnO precursors for AACVD

DOI: 10.1021/acsaelm.9b00190
ACS Appl. Electron. Mater. 2019, 1, 1408−1417

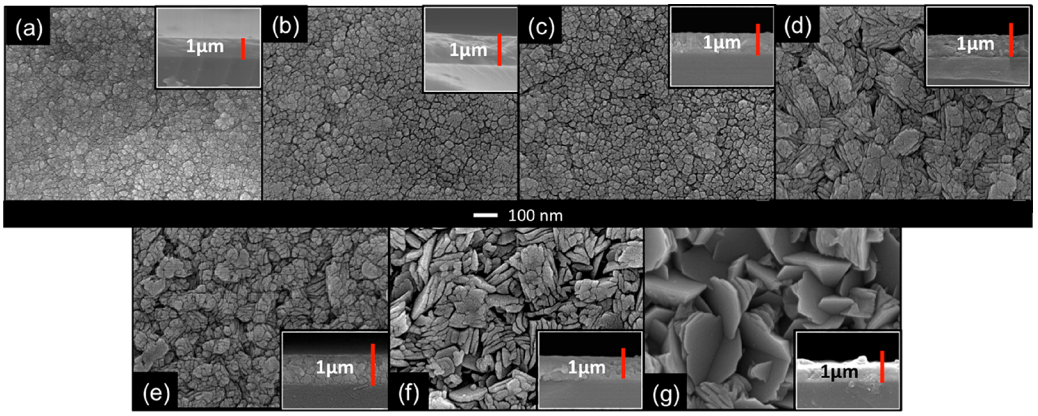

Figure 2. Top-down and side-on (inset) SEM images of ZnO and Cl-doped ZnO films deposited using (a) 0 mol % Cl, (b) 1 mol % Cl, (c) 3 mol % Cl, (d) 5 mol % Cl, (e) 7 mol % Cl, (f) 10 mol % Cl, and (g) 20 mol % Cl.

are diethylzinc, which is highly pyrophoric, and Zn(II) acetylacetonate, which has limited solubility at neutral pH.[36] NH_4Cl is a cheap, abundant, and easy to handle source of Cl. AACVD of Zn(II) acetate dehydrate with varying amounts of NH_4Cl (0−20 mol %) in MeOH at 500 °C were carried out under an atmospheric pressure of N_2. The ZnO:Cl films deposited appear transparent and uncolored with no visible pinhole defects. A full coverage of the substrate was observed with the films strongly adhered to the substrate, passing the "scotch tape" and steel scalpel mechanical tests. The films were stable under ambient conditions after storage for around six months, and they displayed good stability to common solvents such as methanol, isopropanol, acetone, and chloroform. The facile fabrication carried out in this work demonstrates a clear route to industrial scale-up.

Film Characterization. All deposited films were successfully prepared as a wurtzite ZnO phase with no detected impurity phases, as confirmed by XRD analysis (Figure 1a). The variation in preferred orientation was observed as differences in the relative intensity of diffraction peaks between samples. This phenomenon commonly arises as the minimization of internal stress and surface energy occurred during the film growth.[37] The (002) plane preferred orientation observed in the undoped ZnO film is the most condensed and thermodynamically stable plane in the wurtzite structure, as is normally observed in ZnO films.[38] The incorporation of Cl into ZnO resulted in an increasing preference for the (100) plane in the ZnO:Cl films, with the (101) plane becoming ultimately dominant at the highest doping levels. This was also observed in the case of ZnO:Cl films prepared by atomic layer deposition[12] and in ZnO:Cl nanospheres.[39] Preference for the (100) plane orientation is favorable for TCO properties because of the relatively larger grain size compared to that with (002) orientation, which is preferable for piezoelectric applications. The preferred orientation is reported to be a crucial factor for certain applications.[38] Figure 1b illustrates that the cell parameters *a*, *c* and the cell volume of the ZnO films tend to increase with Cl doping, suggesting Cl was incorporated into the ZnO lattice. This effect can be rationalized due to the larger ionic radius of Cl^- (r_i = 1.81 Å) compared with O^{2-} (r_i = 1.40 Å).[40]

X-ray photoelectron spectroscopic (XPS) analysis was used to confirm the chemical components as well as the oxidation states of all elements in the films. High resolution XPS spectra of Zn 2p and O 1s of the ZnO:Cl film from 10 mol % Cl are shown as Figure 1c as a representative. The Zn $2p_{3/2}$ peak at 1020.7 (±0.2) eV can be assigned as the Zn−O bond. The O 1s spectrum can be deconvoluted into two peaks; the peak O_I at 529.7 (±0.2) eV is attributed to O^{2-} in the lattice and the peak O_{II} at 531.5 (±0.2) eV can be identified as O bonded with adventitious C (e.g., C−O, C═O) or loosely bound oxygen species such as adsorbed O_2 and −OH, which is attributed to chemisorption on the surface of the films.[41−44] Both Zn 2p and O 1s spectra of all films were similarly observed. The ratio of Zn to lattice O in the bulk of undoped and Cl doped films was determined from the Zn 2p and O 1s peak areas and was consistently found to be 1.3 to 1. The slight excess of Zn compared to lattice O is attributed to preferential sputtering of O compared to Zn during the etching process. In all Cl-doped films, the Cl $2p_{3/2}$ peak was detected at around 198.3 (±0.2) eV, which can be assigned to the Cl−Zn bond; this is similar to those reported in the literature and supports the conclusion that the Cl dopant is ionic and therefore acting as an electron donor.[12,15,16]

Preferential sputtering of Cl by the Ar^+ ion beam inhibited ion-etch depth profiling of the Cl bulk concentration by XPS (see Supporting Information). A similar effect has previously been observed for other light elements such as F,[9] O,[45] and S.[46] Therefore, SIMS depth profiling was instead used to study the depth distribution of the Zn, O, Cl, and H species in the films. The relative content of H/Zn and Cl/Zn are illustrated in Figure 1d. Adventitious H was detected in the nominally undoped ZnO film. However, adventitious H could not be observed by ToF-SIMS in Cl-doped samples; the reason behind this is unclear, although we suggest that HCl formation may occur preferentially to ZnO:H during deposition in the presence of a Cl source to limit its incorporation into the growing film. Moreover, since contamination by C was only detected in the undoped ZnO, the H is likely to originate from C−H, which corresponds to the C 1s environments observed during XPS depth profiling. The C 1s deconvoluted peak area (Figure 1e) both on the surface and under etching obtained in the undoped ZnO film were higher than those in ZnO:Cl films. The 5 mol % Cl-doped ZnO film was revealed by ToF-SIMS to have consistently high chlorine content throughout its depth (see Figure 1e). This evidence supports the conclusion that etching was preferentially sputtering Cl from the film during XPS depth profiling.

The SEM images shown (Figure 2) demonstrate that all ZnO:Cl films had a dense and highly textured morphology. The films were visibly affected by the addition of 5−10 mol % Cl as the grain size was increased. It was apparent that the grain grows with increasing Cl content, causing an increase in particle size.

DOI: 10.1021/acsaelm.9b00190
ACS Appl. Electron. Mater. 2019, 1, 1408−1417

The grain shape becomes plate-like on increasing the %Cl in the precursor solution to 20 mol %. Meanwhile, side-on SEM micrographs (Figure 2, inset) were used to reveal the thicknesses of the films, which are given in Table 1.

Table 1. Cell Parameters *a*, *c*, Cell Volume *V*, and Film Thickness

	Cell parameters			
mol % Cl	*a* (Å)	*c* (Å)	*V* (Å^3)	Thickness (nm)
0	3.256(11)	5.2067(11)	47.65(3)	930
1	3.2510(4)	5.2123(13)	47.71(1)	950
3	3.2527(1)	5.2115(7)	47.75(1)	630
5	3.2545(1)	5.2118(7)	47.81(1)	650
7	3.2546(2)	5.2138(6)	47.83(1)	650
10	3.2554(1)	5.2176(5)	47.89(1)	760
20	3.2553(5)	5.2156(12)	47.86(2)	600

Figure 3 shows AFM images of undoped ZnO and ZnO:Cl from 7 mol % Cl and the film roughness in the root mean squared (R_q) roughness value. The topology of films changed dramatically upon 7 mol % Cl doping. The undoped ZnO film had an R_q of 13.8 ± 0.2 nm while 7 mol % ZnO:Cl had a higher R_q of 47.1 ± 2.9 nm. This film was therefore almost four times as rough as the undoped ZnO. The change in film topology with doping likely arises from the shift in nanocrystallite preferred orientation and appears to be a strong factor in determining the surface roughness.

Functional Properties. *Electrical Properties.* The electrical resistivity (ρ), carrier concentration (n), and carrier mobility (μ) are shown in Figure 4a and Table 2. The undoped ZnO films exhibited resistivities of 1.4×10^{-1} Ω·cm, which was comparable to values reported previously (1.3×10^{-1} Ω·cm) in ZnO films deposited by the same method and precursors.[47] It has been shown that doping ZnO with Cl decreases the resistivity, giving rise to *n*-type conducting behavior. This is expected due to the donation of electrons from substitutional Cl_O defect sites, which are predicted from DFT computational results as the introduction of a shallow donor level derived primarily from Cl 3s states into the conduction band.[48] This causes the carrier concentration to increase initially with increasing Cl doping; this quantity reaches a maximum value using 5 mol % Cl and drops thereafter due to the falling formation energy of compensating defects such as Zn vacancies (V_{Zn}) as the Fermi level rises, a well-known effect both experimentally and computationally.[47,49]

Charge carrier mobility drops off at heavier doping levels, typically the result of an increase in ionized impurity scattering as Cl_O and V_{Zn} defect density increases. However, the dramatic initial increase in mobility from 4.3 to 26.7 cm^2 V^{-1} s^{-1} between undoped and 5 mol % Cl-doped ZnO is an interesting effect, which we suggest is most likely the product of two effects: first, the strongly increased ZnO:Cl grain size with Cl doping as observed in the SEM micrographs above, which reduces the frequency of grain boundary scattering events thus enabling longer electron relaxation times.[50] Second, the rising Fermi level both enables screening of conduction electrons from interface-localized electron trap states and reduces the energy barrier height at the grain boundary.[51,52] The reduction of electron scattering in general is key to improving carrier mobility[53,54] and the dependence of electron mobility on carrier density in polycrystalline films is evident from Figure 4b.

The film formed from 5 mol % Cl doping exhibited the best electrical properties as a conductor with the lowest electrical resistivity of 2.72×10^{-3} Ω·cm, the highest carrier concentration of 8.58×10^{19} cm^{-3}, and the highest carrier mobility of 26.7 cm^2 V^{-1} s^{-1}. The ZnO:Cl films prepared by AACVD in this work has lower electrical resistivity in comparison to those obtained using atomic layer deposition (ALD) ($\rho = 1.215 \times 10^{-2}$ Ω·cm)[12] and metal−organic CVD (MOCVD) ($\rho = 3.6 \times 10^{-2}$ Ω·cm),[13,14] but higher than that prepared by physical layer deposition (PLD) ($\rho = 6.344 \times 10^{-4}$ Ω·cm).[15,16] Furthermore, the carrier mobility in these ZnO:Cl films were greater than those prepared by MOCVD (μ = 9−14 cm^2 V^{-1} s^{-1})[13,14] and PLD (μ = 23.7 cm^2 V^{-1} s^{-1})[15,16] and particularly the common F-doped SnO_2 (FTO) industrial coatings such as TEC15 (μ = 21 cm^2 V^{-1} s^{-1}).[55] Carrier mobility is considered to be an important factor in lowering electrical resistivity in TCOs when carrier density limits are imposed by the doping regime.[56] This work demonstrates the advantage of anion doping for enhanced carrier mobility compared to cation doping for ZnO; from

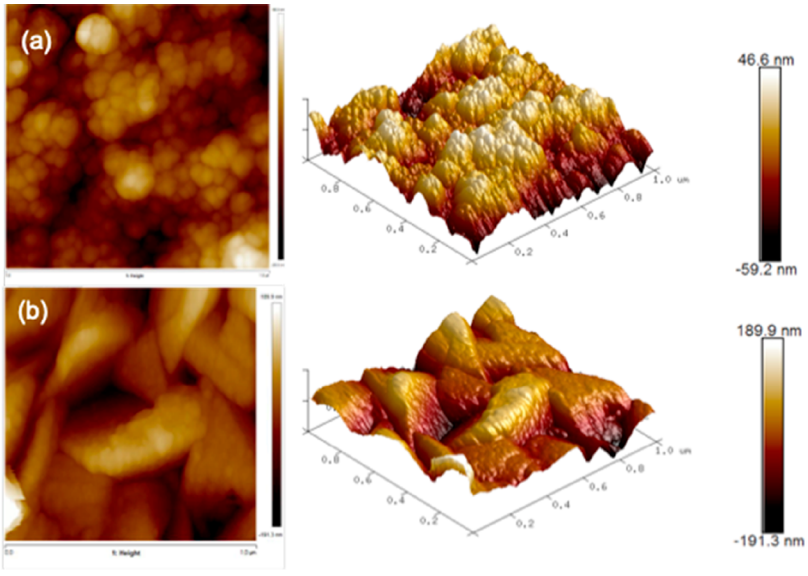

Figure 3. AFM images probed under the area of 1.0 μm × 1.0 μm of (a) ZnO and (b) 7 mol % Cl-doped ZnO films and their 3D image of the same area.

DOI: 10.1021/acsaelm.9b00190
ACS Appl. Electron. Mater. 2019, 1, 1408−1417

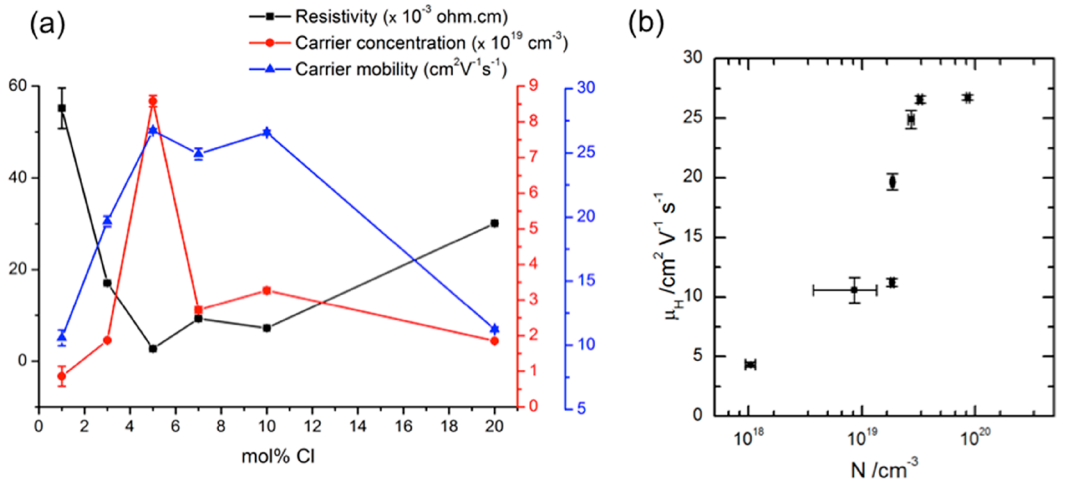

Figure 4. (a) The plot of electrical properties of ZnO:Cl films, including resistivity, carrier concentration, and carrier mobility and (b) the plot of Hall mobility (μ_H) as a function of carrier density (N) were present with average values with standard error bar.

Table 2. Functional Properties of ZnO:Cl Films including TCO Properties and Photocatalytic Properties[a]

	TCO properties						
	Optical properties		Electrical properties				Photocatalytic properties
mol % Cl	$\%T_{\lambda 400-700}$	E_g (eV)	N ($\times 10^{19}$ cm^{-3})	μ_H (cm^2 V^{-1} s^{-1})	ρ ($\times 10^{-3}$ Ω·cm)	R_{sh} (Ω□$^{-1}$)	ξ ($\times 10^{-4}$ molec/photon)
0	68	3.32 ± 0.01	0.10 ± 0.01	4.34 ± 0.12	1400.00 ± 44.97	15053.8 ± 483.6	0.17 ± 0.04
1	69	3.31 ± 0.01	0.86 ± 0.28	15.56 ± 0.61	50.86 ± 4.43	580.7 ± 46.6	0.22 ± 0.06
3	78	3.30 ± 0.01	1.86 ± 0.03	19.67 ± 0.40	17.03 ± 0.14	270.4 ± 2.2	0.39 ± 0.09
5	82	3.30 ± 0.01	8.58 ± 0.16	26.74 ± 0.13	2.72 ± 0.04	41.9 ± 0.7	0.89 ± 0.10
7	80	3.29 ± 0.01	2.72 ± 0.09	24.91 ± 0.44	9.23 ± 0.13	142.0 ± 1.9	1.63 ± 0.03
10	82	3.32 ± 0.01	3.27 ± 0.08	26.58 ± 0.17	7.19 ± 0.15	94.6 ± 2.0	0.51 ± 0.17
20	80	3.31 ± 0.01	1.85 ± 0.03	11.23 ± 0.18	30.12 ± 0.08	502.1 ± 1.4	–

[a] E_g = band gap energy, N = carrier concentration, μ_H = carrier mobility or Hall mobility, ρ = electrical resistivity, R_{sh} = sheet resistance, ξ = quantum yield efficiency.

comparison of ZnO films deposited by AACVD, the carrier mobility of these ZnO:Cl films (5 mol % Cl, μ = 26.74 cm^2 V^{-1} s^{-1}) is excellent compared to the best mobility obtained in cation-doped ZnO films, e.g. Al (μ = 9.3 cm^2 V^{-1} s^{-1}),[57] Ga (μ = 10.1 cm^2 V^{-1} s^{-1}), In (μ = 5.1 cm^2 V^{-1} s^{-1}),[8] Sc (μ = 7.5 cm^2 V^{-1} s^{-1}),[47] Si (μ = 16.5 cm^2 V^{-1} s^{-1}),[36] and well-known anion-doped ZnO films, F (μ = 12.5 cm^2 V^{-1} s^{-1}).[9] The predominant effect of anion doping on carrier mobility can be illustrated when compared with other cation-doped ZnO[8,47] with the same order of resistivity (10^{-3} Ω·cm), which have lower carrier mobilities (<9 cm^2 V^{-1} s^{-1}).

Optical Properties. The transmittance and reflectance spectra of all films are reported in Figure 5a–b. The transmittance of the bare glass in the visible range 400–700 nm ($\%T_{\lambda 400-700}$) is 89%. The undoped ZnO film had some visible carbon contamination, thus resulting in the lowest transparency with $\%T_{\lambda 400-700}$ of 68%. ZnO:Cl films prepared in this work are colorless and became more transparent; the films formed from 5 to 20 mol % Cl have a $\%T_{\lambda 400-700}$ greater than 80% with 5 mol % showing the highest value of 82%.

As all films prepared here behave as a degenerate semiconductor, the band gap was estimated from a correction to the Tauc method to account for underestimation arising from broadening of the initial and final electronic states.[47] In order to do so, a broadening parameter $^{\pi}/_{4}\Gamma$ was obtained from the separation of extrapolations along the edge of α and α^2 plots against $h\nu$ and then the parameter was added to the uncorrected band gap to obtain a corrected estimate, as discussed by Dolgonos et al. (Figure 5d).[58] The absorption coefficient (α) was extracted from the equation: $T/(1-R)^2 = \exp(-\alpha d)$ where T is %transmittance, R is %reflectance, and d is the film thickness.[53] The band gap energy of undoped ZnO obtained in this way was 3.32 ± 0.01 eV, which is similarly observed in other reports (Figure 5c).[12,59] The band gaps were not significantly changed as a function of Cl content from 1 to 20 mol % (Table 2), which were affected by two conflicting factors. First, the raising of the Fermi level with increasing carrier density in TCOs typically widens the optical band gap energy because of the Burstein–Moss effect.[48] Second, doping, particularly degenerate doping, can produce electron–electron and electron–impurity scattering; this phenomenon could narrow the band gap due to the fundamental band gap renormalization (Δ_g^{RN}).[60] The origin of band gap renormalization in heavily doped semiconductors such as ZnO and SnO_2 was discussed.[61] The results obtained imply the competing of both band gap widening and narrowing effects.

Photocatalytic Properties. The photocatalytic properties of films were determined by the degradation of stearic acid under UVA light illumination where the reaction can be explained by the following reaction:

$$CH_3(CH_2)_{16}CO_2H + 26O_2 \xrightarrow{\text{ZnO } (h\nu \geq E_g)} 18CO_2 + 18H_2O \quad (1)$$

The number of stearic acid molecules degraded per incident photon is reported in terms of formal quantum efficiency (ξ).

DOI: 10.1021/acsaelm.9b00190
ACS Appl. Electron. Mater. 2019, 1, 1408–1417

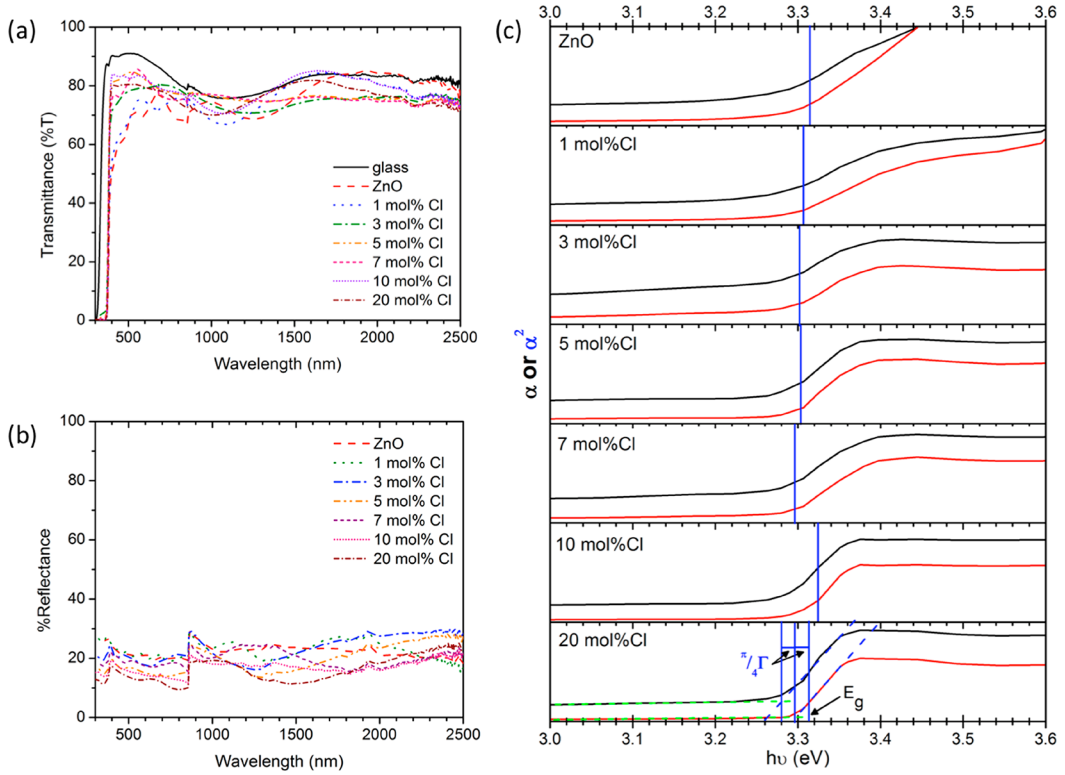

Figure 5. (a) Transmittance and (b) reflectance spectra of all films shown against the spectrum for bare glass as reference. ZnO:Cl films enhance %T from undoped ZnO film, and the most transparent film was obtained from 5 mol % Cl doped ZnO film with a %T of 82. (c) Tauc plot of ZnO film and corrected Tauc plots of Cl-doped ZnO films deposited using 1−20 mol % Cl. The extrapolated lines on *x*-axis show band gap energy (E_g).

According to the plot of ξ (Figure 6), the pure ZnO had a degradation rate of $(0.17 \pm 0.04) \times 10^{-4}$ molecules/photon. In

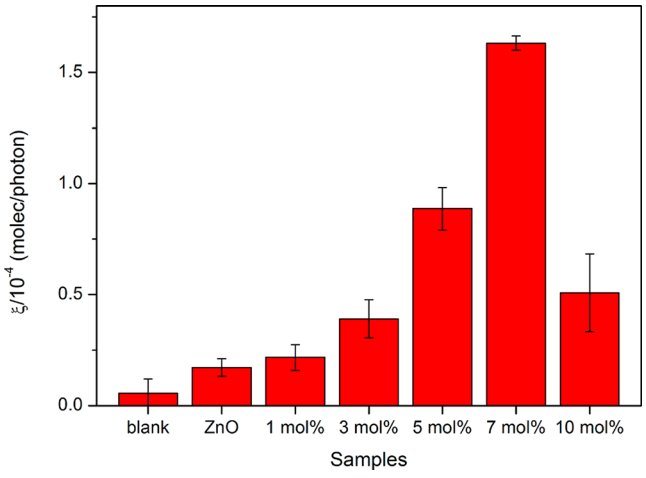

Figure 6. Plot of formal quantum efficiency (ξ) indicating the stearic acid degradation of undoped and ZnO:Cl films under UVA irradiation. The film deposited using 7 mol % Cl shows the highest performance.

ZnO:Cl, ξ gradually increases with Cl concentrations of 1−3 mol % Cl. A significant change can be observed from 5 mol % Cl, and the most distinct value was found for the film formed using 7 mol % Cl with the highest ξ of $(1.63 \pm 0.03) \times 10^{-4}$ molecule/photon, which is about 10 times greater than that of the undoped ZnO film. The photocatalytic activity, however, decreased with a higher Cl concentration in the precursor solution of 10 mol % Cl.

The enhancement in photocatalytic activity of ZnO:Cl thin films could be due to many reasons. The morphology change observed in SEM images is a possible cause of the efficiency enhancement. The higher surface roughness, by approximately four times, of the ZnO:Cl from 7 mol % Cl compared to the pure ZnO could also be an important factor.[62] As electron−hole pair recombination is a competing process causing the drop in photocatalytic efficiency, desirable charge transport properties can prolong the recombination of photogenerated carriers. Exciton effective masses relate the photocatalytic properties to the carrier mobility; e.g. lighter electrons and heavier holes are found to be crucial to separate photoinduced charges.[63,64] It is interesting to note that the ξ value increases almost linearly with carrier concentration and carrier mobility (Figure 7). The electrical properties suggest the increase of both population and mobility of photogenerated carriers could take part in the redox reaction of stearic acid degradation and retards the recombination of electrons and holes.[62] Figure 8 shows the photoluminescence spectra of undoped ZnO and 7 mol % Cl doped ZnO films. The UV emission peaks observed at around 380−390 nm (~3.18−3.26 eV) correspond to near band-edge emission (NBE) of free excitons,[65] slightly red-shifted compared to band gaps determined from absorption spectra due to Stokes shift, in which the photoexcited electron undergoes some nonradiative energy loss before returning to the VB.[66] The green emission band contoured at around 550 nm (~2.25 eV) could originate from deep-level defects, which are most likely to be oxygen vacancies as it has the lowest formation energy under oxygen-deficient condition.[39,47,67] This broad green emission band showing some shoulders could be composed of some emission peaks, suggesting the multiple radiative emission from several substates of shallow donor levels to a deeply trapped state

DOI: 10.1021/acsaelm.9b00190
ACS Appl. Electron. Mater. 2019, 1, 1408−1417

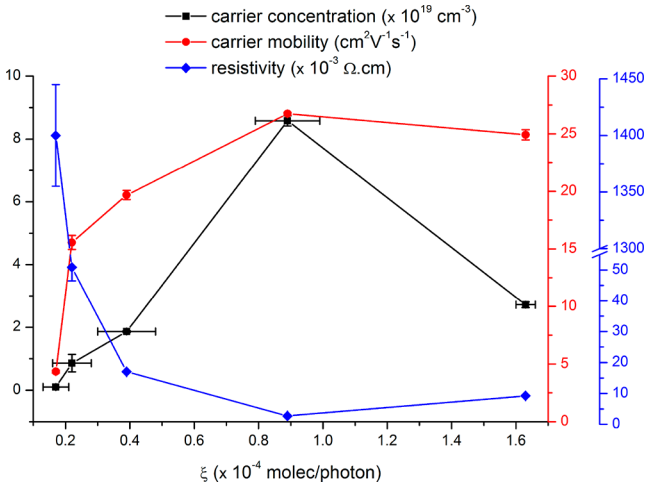

Figure 7. Plot of electrical properties as a function of formal quantum efficiency (ξ).

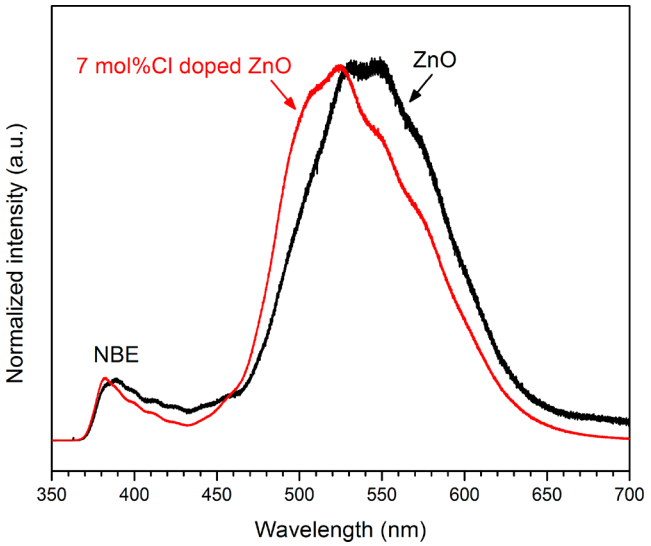

Figure 8. Photoluminescence spectra of undoped ZnO film and 7 mol % Cl doped ZnO film. NBE refers to near band-edge emission.

of V_o^{++}.[68] The shift of this band in 7 mol % Cl-doped ZnO film to a shorter wavelength implies that higher energy required for photoexcited electrons to recombine with holes via trapping deep-level defect states,[67] suggesting that the improvement in photocatalytic efficiency of the ZnO film deposited using 7 mol % Cl.

We have shown the potential of the AACVD method that can be tuned to produce cost-effective multifunctional films by the choice of precursors. The use of NH_4Cl, instead of $FeCl_3$ used in previous work, resulted in a simpler and cheaper film deposition route with the elimination of solid waste products while producing an enhancement in electrical properties. Optimum Cl concentrations were found for the three key material properties of transparency, electrical conductivity, and photocatalytic activity. This cost-effective route provides a one-step deposition onto inexpensive glass substrates without further postdeposition treatment as routinely required in other film deposition techniques such as atomic layer deposition (ALD), RF magnetron sputtering (rf-MS), and molecular beam epitaxy (MBE). The ZnO:Cl thin films produced here show promise for various electronic and energy-efficient applications. The scope of applications is expanded because the AACVD technique has been used to tune the macroscopic properties of the films through control over their microscopic morphology and surface roughness.

CONCLUSIONS

Transparent and electrically conducting ZnO:Cl thin films with demonstrable photocatalytic activity have been fabricated by AACVD. Cl was successfully substituted at the O site as evident from an increase in the unit cell parameters and compositional study from XPS and SIMS analyses. SEM images illustrated the influence of Cl doping on the ZnO thin film morphologies. The optical transmittance in the visible region (400−700 nm) was improved by Cl doping, which exceeded 80% in the 5−10 mol % doping range, resulting in transparent and colorless films. All Cl-doped films were electrically conductive as a result of the introduced donor electrons from Cl. A dopant quantity of 5 mol % Cl yielded conducting behavior with a minimum measured resistivity of $(2.72 \pm 0.04) \times 10^{-3}$ Ω·cm, in which the charge carrier concentration and mobility were measured at $(8.58 \pm 0.16) \times 10^{19}$ cm^{-3} and (26.74 ± 0.13) cm^2 V^{-1} s^{-1} respectively, corresponding to a sheet resistance (R_{sh}) of 41.9 $\Omega\square^{-1}$ at a thickness of 650 nm. It clearly represents an approximately 6-fold increase in carrier mobility over the undoped ZnO film, an effect ascribed in part to the significant increase in ZnO grain size when grown in the presence of NH_4Cl. The photocatalytic behavior of the ZnO:Cl films by stearic acid degradation under UVA irradiation was also observed in the films deposited using 7 mol % Cl, yielding the highest formal quantum efficiency (ξ) measured at $(1.63 \pm 0.03) \times 10^{-4}$ molecule/photon. Atomic force microscopy revealed the surface roughness of the films deposited from 7 mol % Cl to be about four times larger than that of undoped ZnO films. The increase in surface roughness, carrier density, and mobility as well as the shift of the photoluminescence deep-level defect emission peak to a shorter wavelength suggest that these were the major factors accountable for the improvement in photocatalytic activity.

ASSOCIATED CONTENT

Supporting Information

The Supporting Information is available free of charge on the ACS Publications website at DOI: 10.1021/acsaelm.9b00190.

XPS analysis for at.%Cl in films, stearic acid degradation test, photoinduced wettability test (PDF)

AUTHOR INFORMATION

Corresponding Author

*E-mail: c.j.carmalt@ucl.ac.uk.

ORCID

Arreerat Jiamprasertboon: 0000-0002-8397-1149
Sebastian C. Dixon: 0000-0002-6936-0499
Sanjayan Sathasivam: 0000-0002-5206-9558
Michael J. Powell: 0000-0003-2453-9134
Yao Lu: 0000-0001-9566-4122
Claire J. Carmalt: 0000-0003-1788-6971

Notes

The authors declare no competing financial interest.

ACKNOWLEDGMENTS

The Development and Promotion of Science and Technology Talents Project (DPST) is acknowledged for the support of A.J.

DOI: 10.1021/acsaelm.9b00190
ACS Appl. Electron. Mater. 2019, 1, 1408−1417

The authors would like to thank NSG Pilkington Glass Ltd. and the Engineering and Physical Sciences Research Council for provision of substrates and for studentship funding for S.C.D. through the M^{3}S Doctoral Training Centre (Grant EP/G036675) and also for Grant EP/N01572X/1. Y.L. acknowledges support from EPSRC Project EP/N024915/1.

REFERENCES

(1) Powell, M. J.; Carmalt, C. J. Aerosols: A Sustainable Route to Functional Materials. *Chem. - Eur. J.* **2017**, *23* (62), 15543−15552.
(2) Hass, G.; Francombe, M. H.; Hoffman, R. W. *Physics of Thin Films: Advances in Research and Development*; Elsevier: 2013.
(3) Kafizas, A.; Noor, N.; Carmichael, P.; Scanlon, D. O.; Carmalt, C. J.; Parkin, I. P. Combinatorial Atmospheric Pressure Chemical Vapor Deposition of F:TiO_2; The Relationship between Photocatalysis and Transparent Conducting Oxide Properties. *Adv. Funct. Mater.* **2014**, *24* (12), 1758−1771.
(4) Bhachu, D. S.; Sathasivam, S.; Sankar, G.; Scanlon, D. O.; Cibin, G.; Carmalt, C. J.; Parkin, I. P.; Watson, G. W.; Bawaked, S. M.; Obaid, A. Y.; et al. Solution Processing Route to Multifunctional Titania Thin Films: Highly Conductive and Photcatalytically Active Nb:TiO_2. *Adv. Funct. Mater.* **2014**, *24* (32), 5075−5085.
(5) Bawaked, S. M.; Sathasivam, S.; Bhachu, D. S.; Chadwick, N.; Obaid, A. Y.; Al-Thabaiti, S.; Basahel, S. N.; Carmalt, C. J.; Parkin, I. P. Aerosol Assisted Chemical Vapor Deposition of Conductive and Photocatalytically Active Tantalum Doped Titanium Dioxide Films. *J. Mater. Chem. A* **2014**, *2* (32), 12849.
(6) Sathasivam, S.; Bhachu, D. S.; Lu, Y.; Chadwick, N.; Althabaiti, S. A.; Alyoubi, A. O.; Basahel, S. N.; Carmalt, C. J.; Parkin, I. P. Tungsten Doped TiO_2 with Enhanced Photocatalytic and Optoelectrical Properties via Aerosol Assisted Chemical Vapor Deposition. *Sci. Rep.* **2015**, *5* (1), 10952.
(7) Morgan, B. J.; Scanlon, D. O.; Watson, G. W. Small Polarons in Nb- and Ta-Doped Rutile and Anatase TiO_2. *J. Mater. Chem.* **2009**, *19* (29), 5175.
(8) Potter, D. B.; Bhachu, D. S.; Powell, M. J.; Darr, J. A.; Parkin, I. P.; Carmalt, C. J. Al-, Ga-, and In-Doped ZnO Thin Films via Aerosol Assisted CVD for Use as Transparent Conducting Oxides. *Phys. Status Solidi A* **2016**, *213* (5), 1346−1352.
(9) Ponja, S. D.; Sathasivam, S.; Parkin, I. P.; Carmalt, C. J. Transparent Conductive Aluminium and Fluorine Co-Doped Zinc Oxide Films via Aerosol Assisted Chemical Vapour Deposition. *RSC Adv.* **2014**, *4* (91), 49723−49728.
(10) Gordon, R. G. Criteria for Choosing Transparent Conductors. *MRS Bull.* **2000**, *25* (08), 52−57.
(11) Rousset, J.; Saucedo, E.; Lincot, D. Extrinsic Doping of Electrodeposited Zinc Oxide Films by Chlorine for Transparent Conductive Oxide Applications Extrinsic Doping of Electrodeposited Zinc Oxide Films by Chlorine for Transparent Conductive Oxide Applications. *Chem. Mater.* **2009**, *21* (3), 534−540.
(12) Choi, Y.-J.; Kang, K.-M.; Lee, H.-S.; Park, H.-H. Non-Laminated Growth of Chlorine-Doped Zinc Oxide Films by Atomic Layer Deposition at Low Temperatures. *J. Mater. Chem. C* **2015**, *3* (32), 8336−8343.
(13) Chikoidze, E.; Nolan, M.; Modreanu, M.; Sallet, V.; Galtier, P. Effect of Chlorine Doping on Electrical and Optical Properties of ZnO Thin Films. *Thin Solid Films* **2008**, *516* (22), 8146−8149.
(14) Chikoidze, E.; Modreanu, M.; Sallet, V.; Gorochov, O.; Galtier, P. Electrical Properties of Chlorine-Doped ZnO Thin Films Grown by MOCVD. *Phys. Status Solidi A* **2008**, *205* (7), 1575−1579.
(15) Lee, J.; Park, E.; Subramaniam, N. G.; Lee, J.; Lee, J.; Lee, J.; Kang, T. Non-Metallic Element (Chlorine) Doped Zinc Oxide Grown by Pulsed Laser Deposition for Application in Transparent Electrode. *Curr. Appl. Phys.* **2012**, *12* (SUPPL.4), S80−S84.
(16) Lee, J. C.; Subramaniam, N. G.; Lee, J. W.; Lee, J. C.; Kang, T. W. Evaluation of Optimal Chlorine Doping Concentration in Zinc Oxide on Glass for Application as New Transparent Conductive Oxide. *Phys. Status Solidi A* **2013**, *210* (12), 2638−2643.
(17) Lee, K. M.; Lai, C. W.; Ngai, K. S.; Juan, J. C. Recent Developments of Zinc Oxide Based Photocatalyst in Water Treatment Technology: A Review. *Water Res.* **2016**, *88*, 428−448.
(18) Gao, W.; Li, Z. ZnO Thin Films Produced by Magnetron Sputtering. *Ceram. Int.* **2004**, *30* (7), 1155−1159.
(19) Craciun, V.; Elders, J.; Gardeniers, J. G. E.; Boyd, I. W. Characteristics of High Quality ZnO Thin Films Deposited by Pulsed Laser Deposition. *Appl. Phys. Lett.* **1994**, *65* (23), 2963−2965.
(20) Ilican, S.; Caglar, Y.; Caglar, M. Preparation and Characterization of ZnO Thin Films Deposited by Sol-Gel Spin Coating Method. *J. Optoelectron. Adv. Mater.* **2008**, *10*, 2578−2583.
(21) Carcia, P. F.; McLean, R. S.; Reilly, M. H. High-Performance ZnO Thin-Film Transistors on Gate Dielectrics Grown by Atomic Layer Deposition. *Appl. Phys. Lett.* **2006**, *88* (12), 123509−123509−3.
(22) Dixon, S. C.; Jiamprasertboon, A.; Carmalt, C. J.; Parkin, I. P. Luminescence Behaviour and Deposition of Sc_2O_3 Thin Films from Scandium(III) Acetylacetonate at Ambient Pressure. *Appl. Phys. Lett.* **2018**, *112* (22), 221902−221902−5.
(23) Dixon, S. C.; Peveler, W. J.; Noor, N.; Bear, J. C.; Parkin, I. P. Superhydrophobic Au/Polymer Nanocomposite Films via AACVD/Swell Encapsulation Tandem Synthesis Procedure. *RSC Adv.* **2016**, *6* (37), 31146−31152.
(24) Zhuang, A.; Liao, R.; Dixon, S. C.; Lu, Y.; Sathasivam, S.; Parkin, I. P.; Carmalt, C. J. Transparent Superhydrophobic PTFE Films via One-Step Aerosol Assisted Chemical Vapor Deposition. *RSC Adv.* **2017**, *7* (47), 29275−29283.
(25) Zhuang, A.; Liao, R.; Lu, Y.; Dixon, S. C.; Jiamprasertboon, A.; Chen, F.; Sathasivam, S.; Parkin, I. P.; Carmalt, C. J. Transforming a Simple Commercial Glue into Highly Robust Superhydrophobic Surfaces via Aerosol-Assisted Chemical Vapor Deposition. *ACS Appl. Mater. Interfaces* **2017**, *9* (48), 42327−42335.
(26) Marchand, P.; Hassan, I. A.; Parkin, I. P.; Carmalt, C. J. Aerosol-Assisted Delivery of Precursors for Chemical Vapour Deposition: Expanding the Scope of CVD for Materials Fabrication. *Dalton Trans.* **2013**, *42* (26), 9406−9422.
(27) Knapp, C. E.; Carmalt, C. J. Solution Based CVD of Main Group Materials. *Chem. Soc. Rev.* **2016**, *45* (4), 1036−1064.
(28) Choy, K. L. Chemical Vapour Deposition of Coatings. *Prog. Mater. Sci.* **2003**, *48* (2), 57−170.
(29) Hou, X.; Choy, K.-L. Processing and Applications of Aerosol-Assisted Chemical Vapor Deposition. *Chem. Vap. Deposition* **2006**, *12* (10), 583−596.
(30) Xu, C.; Hampden-Smith, M. J.; Kodas, T. T. Aerosol-Assisted Chemical Vapor Deposition (AACVD) of Binary Alloy (Ag_xPd_{1-x}, Cu_xPd_{1-x}, Ag_xCu_{1-x}) Films and Studies of Their Compositional Variation. *Chem. Mater.* **1995**, *7* (8), 1539−1546.
(31) Waugh, M. R.; Hyett, G.; Parkin, I. P. Zinc Oxide Thin Films Grown by Aerosol Assisted CVD. *Chem. Vap. Deposition* **2008**, *14* (11−12), 366−372.
(32) Powell, M. J.; Potter, D. B.; Wilson, R. L.; Darr, J. A.; Parkin, I. P.; Carmalt, C. J. Scaling Aerosol Assisted Chemical Vapour Deposition: Exploring the Relationship between Growth Rate and Film Properties. *Mater. Des.* **2017**, *129*, 116−124.
(33) Jiamprasertboon, A.; Powell, M. J.; Dixon, S. C.; Quesada-Cabrera, R.; Alotaibi, A. M.; Lu, Y.; Zhuang, A.; Sathasivam, S.; Siritanon, T.; Parkin, I. P. Photocatalytic and Electrically Conductive Transparent Cl-Doped ZnO Thin Films via Aerosol-Assisted Chemical Vapour Deposition. *J. Mater. Chem. A* **2018**, *6* (26), 12682−12692.
(34) C. Larson, A.; B. Von Dreele, R. General Structure Analysis System (GSAS). *Structure* **2004**, *748* (LAUR 86−748), 86−748.
(35) Toby, B. H. EXPGUI, a Graphical User Interface for GSAS. *J. Appl. Crystallogr.* **2001**, *34* (2), 210−213.
(36) Potter, D. B.; Powell, M. J.; Darr, J. A.; Parkin, I. P.; Carmalt, C. J. Transparent Conducting Oxide Thin Films of Si-Doped ZnO Prepared by Aerosol Assisted CVD. *RSC Adv.* **2017**, *7* (18), 10806−10814.
(37) Bao, D.; Gu, H.; Kuang, A. Sol-Gel-Derived c-Axis Oriented Z, QO Thin Films. *Thin Solid Films* **1998**, *312* (X), 37−39.

DOI: 10.1021/acsaelm.9b00190
ACS Appl. Electron. Mater. 2019, 1, 1408−1417

(38) Ko Park, S.-H.; Lee, Y. E. Controlling Preferred Orientation of ZnO Thin Films by Atomic Layer Deposition. *J. Mater. Sci.* **2004**, *39* (6), 2195−2197.
(39) Tao, Z.; Yu, X.; Fei, X.; Liu, J.; Yang, G.; Zhao, Y.; Yang, S.; Yang, L. Synthesis and Photoluminescence of Cl-Doped ZnO Nanospheres. *Opt. Mater. (Amsterdam, Neth.)* **2008**, *31* (1), 1−5.
(40) Shannon, R. D. Revised Effective Ionic Radii and Systematic Studies of Interatomic Distances in Halides and Chalcogenides. *Acta Crystallogr., Sect. A: Cryst. Phys., Diffr., Theor. Gen. Crystallogr.* **1976**, *32* (5), 751−767.
(41) Mar, L. G.; Timbrell, P. Y.; Lamb, R. N. An XPS Study of Zinc-Oxide Thin-Film Growth on Copper Using Zinc Acetate as a Precursor. *Thin Solid Films* **1993**, *223* (2), 341−347.
(42) Chen, M.; Wang, X.; Yu, Y. H.; Pei, Z. L.; Bai, X. D.; Sun, C.; Huang, R. F.; Wen, L. S. X-Ray Photoelectron Spectroscopy and Auger Electron Spectroscopy Studies of Al-Doped ZnO Films. *Appl. Surf. Sci.* **2000**, *158* (1), 134−140.
(43) Park, J.-W.; So, H. S.; Lee, H.-M.; Kim, H.-J.; Kim, H.-K.; Lee, H. Transition from a Nanocrystalline Phase to an Amorphous Phase in In-Si-O Thin Films: The Correlation between the Microstructure and the Optical Properties. *J. Appl. Phys.* **2015**, *117* (15), 155305.
(44) Islam, M. N.; Ghosh, T. B.; Chopra, K. L.; Acharya, H. N. XPS and X-Ray Diffraction Studies of Aluminum-Doped Zinc Oxide Transparent Conducting Films. *Thin Solid Films* **1996**, *280* (1−2), 20−25.
(45) Xue, H.; Chen, Y.; Xu, X. L.; Zhang, G. H.; Zhang, H.; Ma, S. Y. X-Ray Diffraction Spectroscopy and X-Ray Photoelectron Spectroscopy Studies of Cu-Doped ZnO Films. *Phys. E* **2009**, *41* (5), 788−791.
(46) Simpson, R.; White, R. G.; Watts, J. F.; Baker, M. A. XPS Investigation of Monatomic and Cluster Argon Ion Sputtering of Tantalum Pentoxide. *Appl. Surf. Sci.* **2017**, *405*, 79−87.
(47) Baker, M. A.; Gilmore, R.; Lenardi, C.; Gissler, W. XPS Investigation of Preferential Sputtering of S from MoS2and Determination of MoSxstoichiometry from Mo and S Peak Positions. *Appl. Surf. Sci.* **1999**, *150* (1), 255−262.
(48) Dixon, S. C.; Sathasivam, S.; Williamson, B. A. D.; Scanlon, D. O.; Carmalt, C. J.; Parkin, I. P. Transparent Conducting N-Type ZnO:Sc - Synthesis, Optoelectronic Properties and Theoretical Insight. *J. Mater. Chem. C* **2017**, *5* (30), 7585−7597.
(49) Slassi, A. First-Principles and Boltzmann Equation Studies of the Cl-Doped ZnO Transparent Conducting Oxide. *Optik (Munich, Ger.)* **2015**, *126* (23), 4751−4756.
(50) Lany, S.; Zunger, A. Dopability, Intrinsic Conductivity, and Nonstoichiometry of Transparent Conducting Oxides. *Phys. Rev. Lett.* **2007**, *98* (4), 045501.
(51) Wu, H. W.; Yang, R. Y.; Hsiung, C. M.; Chu, C. H. Influence of Ag Thickness of Aluminum-Doped ZnO/Ag/Aluminum-Doped ZnO Thin Films. *Thin Solid Films* **2012**, *520* (24), 7147−7152.
(52) Cornelius, S.; Vinnichenko, M. Al in ZnO — From Doping to Alloying: An Investigation of Al Electrical Activation in Relation to Structure and Charge Transport Limits. *Thin Solid Films* **2016**, *605*, 20−29.
(53) Bikowski, A.; Ellmer, K. Analytical Model of Electron Transport in Polycrystalline, Degenerately Doped ZnO Films. *J. Appl. Phys.* **2014**, *116* (14), 143704.
(54) Pei, Z. L.; Sun, C.; Tan, M. H.; Xiao, J. Q.; Guan, D. H.; Huang, R. F.; Wen, L. S. Optical and Electrical Properties of Direct-Current Magnetron Sputtered ZnO:Al Films. *J. Appl. Phys.* **2001**, *90* (7), 3432−3436.
(55) Dixon, S. C.; Scanlon, D. O.; Carmalt, C. J.; Parkin, I. P. N-Type Doped Transparent Conducting Binary Oxides: An Overview. *J. Mater. Chem. C* **2016**, *4* (29), 6946−6961.
(56) Noor, N.; Parkin, I. P. Enhanced Transparent-Conducting Fluorine-Doped Tin Oxide Films Formed by Aerosol-Assisted Chemical Vapour Deposition. *J. Mater. Chem. C* **2013**, *1* (5), 984−996.
(57) Shanthi, S.; Subramanian, C.; Ramasamy, P. Growth and Characterization of Antimony Doped Tin Oxide Thin Films. *J. Cryst. Growth* **1999**, *197* (4), 858−864.
(58) Manzi, J. A.; Knapp, C. E.; Parkin, I. P.; Carmalt, C. J. Aerosol Assisted Chemical Vapour Deposition of Transparent Conductive Aluminum-Doped Zinc Oxide Thin Films from a Zinc Triflate Precursor. *Thin Solid Films* **2016**, *616*, 477−481.
(59) Dolgonos, A.; Mason, T. O.; Poeppelmeier, K. R. Direct Optical Band Gap Measurement in Polycrystalline Semiconductors: A Critical Look at the Tauc Method. *J. Solid State Chem.* **2016**, *240*, 43−48.
(60) Gupta, T. K. Application of Zinc Oxide Varistors. *J. Am. Ceram. Soc.* **1990**, *73* (7), 1817−1840.
(61) Berggren, K. F.; Sernelius, B. E. Band-Gap Narrowing in Heavily Doped Many-Valley Semiconductors. *Phys. Rev. B: Condens. Matter Mater. Phys.* **1981**, *24* (4), 1971−1986.
(62) Walsh, A.; Da Silva, J. L. F.; Wei, S.-H. Origins of Band-Gap Renormalization in Degenerately Doped Semiconductors. *Phys. Rev. B: Condens. Matter Mater. Phys.* **2008**, *78* (7), 075211−075211−5.
(63) Ray, C.; Pal, T. Recent Advances of Metal-Metal Oxide Nanocomposites and Their Tailored Nanostructures in Numerous Catalytic Applications. *J. Mater. Chem. A* **2017**, *5* (20), 9465−9487.
(64) Yu, W.; Zhang, J.; Peng, T. New Insight into the Enhanced Photocatalytic Activity of N-, C- and S-Doped ZnO Photocatalysts. *Appl. Catal., B* **2016**, *181*, 220−227.
(65) Oshikiri, M.; Boero, M.; Ye, J.; Zou, Z.; Kido, G. Electronic Structures of Promising Photocatalysts $InMO_4$ (M = V, Nb, Ta) and $BiVO_4$ for Water Decomposition in the Visible Wavelength Region. *J. Chem. Phys.* **2002**, *117* (15), 7313−7318.
(66) Hu, J. Q.; Bando, Y. Growth and Optical Properties of Single-Crystal Tubular ZnO Whiskers. *Appl. Phys. Lett.* **2003**, *82* (9), 1401−1403.
(67) Shriver, D.; Weller, M.; Overton, T.; Rourke, J.; Armstrong, F. *Inorganic Chemistry*, 6th ed.; W. H. Freeman and Company: 2014.
(68) Sun, W.-C.; Yeh, Y.-C.; Ko, C.-T.; He, H.; Chen, M.-J. Improved Characteristics of Near-Band-Edge and Deep-Level Emissions from ZnO Nanorod Arrays by Atomic-Layer-Deposited Al_2O_3 and ZnO Shell Layers. *Nanoscale Res. Lett.* **2011**, *6* (1), 556.
(69) Liu, D.; Lv, Y.; Zhang, M.; Liu, Y.; Zhu, Y.; Zong, R.; Zhu, Y. Defect-Related Photoluminescence and Photocatalytic Properties of Porous ZnO Nanosheets. *J. Mater. Chem. A* **2014**, *2* (37), 15377.

DOI: 10.1021/acsaelm.9b00190
ACS Appl. Electron. Mater. 2019, 1, 1408−1417